Journal for ImmunoTherapy of Cancer

Engineered red blood cell extracellular vesicles for delivery of Dox and siIDO1 enhance targeted chemo-immunotherapy of acute myeloid leukemia

Yongcan Liu,[1] Jiayuan Hu,[1] Yan Shu,[2] Genyou Li,[1] Fangfang Jin,[1] Jun Ren,[1] Jing Yang,[1] Can Lin,[1] Lisha Tang,[1] Xingyu Wei,[1] Minghui Sun,[1] Xinyi Chen,[1] Nan Wu,[1] Zesong Yang,[3] Ziwei Li,[2] Ling Zhang [1]

To cite: Liu Y, Hu J, Shu Y, *et al*. Engineered red blood cell extracellular vesicles for delivery of Dox and siIDO1 enhance targeted chemo-immunotherapy of acute myeloid leukemia. *Journal for ImmunoTherapy of Cancer* 2025;**13**:e011148. doi:10.1136/jitc-2024-011148

► Additional supplemental material is published online only. To view, please visit the journal online (https://doi.org/10.1136/jitc-2024-011148).

YL, JH and YS contributed equally.

Accepted 28 June 2025

For numbered affiliations see end of article.

Correspondence to
Dr Ling Zhang;
lingzhang@cqmu.edu.cn

Ziwei Li;
liziwei1989@cqu.edu.cn

ABSTRACT

Background As a malignancy of hematopoietic origin, the standard-of-care cytoreductive chemotherapy can not provide satisfactory treatment effect for patients with acute myeloid leukemia (AML). Immunotherapy has received increasing attention in leukemia treatment. However, the immunosuppressive microenvironment and low cancer immunogenicity of AML blasts create major obstacles to effectively inducing immune responses.

Methods We developed an extracellular vesicle-based dual-delivery biosystem, which enhanced anti-AML immune responses by activating the immunogenicity of leukemia cells and relieving immunosuppression in AML allografted mice. Red blood cell-derived extracellular vesicles (REVs) were selected as delivery carriers due to the excellent biocompatibility. REVs were ligated with leukemia-targeting peptide P9 and subsequently loaded with immunogenic cell death (ICD) inducer (Doxorubicin, Dox) and indoleamine 2,3-dioxygenase-1 siRNA (siIDO1) to construct a chemoimmunological cascade biosystem (REVs-Dox/siIDO1-P9).

Results The biosystem can specifically deliver the loaded Dox and siIDO1 into target leukemia cells and was validated capable of inducing efficient ICD. ICD-mediated release of damage-associated molecular patterns synergistically functions with siIDO1-mediated IDO1 silence to effectually recruit $CD8^+$ T cells and enhance $CD8^+$ T cell's functions. In the AML mouse model, REVs-Dox/siIDO1-P9 can evoke a strong antileukemia response and prolong leukemia-bearing mice survival compared with REVs-Dox/siNC-P9 and REVs-siIDO1-P9.

Conclusion Our findings indicate that the extracellular vesicle-based chemoimmunological cascade biosystem provides a novel strategy for AML treatment.

WHAT IS ALREADY KNOWN ON THIS TOPIC

⇒ The standard-of-care cytoreductive chemotherapy can not provide satisfactory treatment effect for patients with acute myeloid leukemia (AML).

⇒ Despite the clinical potential of immunotherapy for AML, its effectiveness is constrained by the dual challenges of immunosuppressive niches and tumor-intrinsic low immunogenicity.

WHAT THIS STUDY ADDS

⇒ This study revealed that red blood cell-derived extracellular vesicles (REVs)-Doxorubicin (Dox)/indoleamine 2,3-dioxygenase-1 siRNA (siIDO1)-P9, an extracellular vesicle-based dual-delivery biosystem, could specifically deliver the loaded Dox (immunogenic cell death inducer) and siIDO1 into target leukemia cells.

⇒ In the AML mouse model, REVs-Dox/siIDO1-P9 was validated as capable of activating the immunogenicity of leukemia cells and relieving immunosuppression within the tumor microenvironment, evoking strong anti-AML immune responses and prolonging leukemia-bearing mice survival.

HOW THIS STUDY MIGHT AFFECT RESEARCH, PRACTICE OR POLICY

⇒ This study elucidates the critical role of chemo-immunotherapy in enhancing anti-AML immune responses and provides a novel therapeutic strategy for this disease.

INTRODUCTION

Acute myeloid leukemia (AML) is a hematological malignancy, featuring an overall 5-year survival rate of approximately 29%.[1] Currently, combination chemotherapy is the standard care for inducing complete remission in AML, but its curative success is limited.[2] Therefore, there is an urgent need to develop alternative, more effective treatment strategies for AML.

Immunotherapy, which harnesses the patient's immune response, has brought about a revolution in cancer treatment over the past decades.[3 4] Myeloblasts in AML are susceptible to the graft-versus-leukemia effect observed with allogeneic hematopoietic stem cell transplantation,[5] suggesting potential for leveraging the immune system to eradicate these cells. However, AML-associated

myeloblasts typically exhibit low mutational burdens, weak stimulation of host immune cells, and mechanisms that inhibit effector T cell responses.[6] Recent findings found that serum amyloid A (SAA) derived from osteoblasts could induce leukemia cells to upregulate indoleamine 2,3-dioxygenase-1 (IDO1) expression, a key enzyme in catalytic conversion of L-tryptophan (L-Trp) into Kynurenine (Kyn).[7 8] This metabolic shift towards L-Trp deficiency and Kyn accumulation suppressed the activity of cytotoxic T lymphocytes (CTLs) and facilitated immunosuppressive regulatory T cell proliferation.[9 10] The SAA-IDO1 axis supported leukemia progression by enhancing Kyn secretion and facilitating immune evasion. Despite favorable outcomes with IDO inhibitors,[11–13] many patients obtain only limited benefit due to the tumor's low immunogenicity and inadequate immune cell infiltration, resulting in suboptimal immune therapy effects.[14 15] Thus, strategies enhancing immunogenicity and immune cell infiltration are essential to broaden the patient population benefiting from IDO1 inhibition therapy.

Immunogenic cell death (ICD), a specialized form of cancer cell death, enhances tumor antigen presentation by releasing damage-associated molecular patterns (DAMPs) such as surface-calreticulin (CRT), extracellular ATP, and high mobility group box 1 (HMGB1).[16] The ICD cascade augments dendritic cells (DCs) maturation and CTLs recruitment in the tumor microenvironment.[17] Studies have shown that chemotherapeutic agents such as Doxorubicin (Dox) can induce ICD, thereby boosting tumor-specific immune responses.[18] Therefore, Dox combined with IDO inhibitors may not only directly kill AML cells but also enhance antigen release, potentially shifting the immune balance from immunosuppression to anti-AML immunity. Taking the above considerations into account, developing a multifunctional platform to integrate chemotherapy and immunotherapy is crucial for advancing effective AML treatment.

Our previous study showed that, as important mediators of intercellular communication, extracellular vesicles (EVs) could transfer nucleic acid contents between leukemia cells and $CD8^+$ T cells, making them promising as drug delivery carriers.[19] It is well established that red blood cell-derived extracellular vesicles (REVs) not only feature safety, versatility, and easy accessibility, but also demonstrate intrinsic liver-targeting properties.[20 21] Liver infiltration of leukemia cells occurs in over 75% of patients with AML.[22] Therefore, REVs have considerable potential in AML treatment applications.[23] Notably, leukemia cells with disseminated nature are exposed to other extramedullary sites, including peripheral blood and spleen.[22] Targeted delivery by EVs has shown significant advantages by increasing delivery efficacy and extending drug retention at the disease site.[24] Through genetic engineering and chemical modification, peptides or protein motifs can be integrated on the surface of EVs, enabling cell-targeting capabilities.[25 26] For instance, 1,2-distearoyl-sn-glycero-3-phosphoethanolamine-polyethylene glycol (DSPE-PEG) has been used to functionalize cell-targeting motifs on exosome surfaces.[27] Previous studies have confirmed that C-type lectin-like molecule-1 (CLL-1) is highly expressed on the cell membrane of leukemia cells and $CD34^+CD38^-$ leukemogenic stem cells rather than on $CD34^+CD38^-$ hematopoietic stem cells.[28] The targeting peptide CDLRSAAVC (named P9), which binds to CLL-1, imparts leukemia-specific targeting properties to nanoparticles, facilitating drug delivery and AML treatment.[28] It is expected that the engineered REVs would use their high biocompatibility and targeting behavior to reduce the leukemic burden in both intramedullary and extramedullary organs, achieving a desirable AML treatment effect that eradicates tumors and boosts immune function.

Here, we developed a REVs-based biosystem co-delivering Dox and siIDO1, named as REVs-Dox/siIDO1-P9, for chemoimmunological cascade therapy of AML. Functionalized on the surface of REVs, targeting peptide P9 enabled REVs-Dox/siIDO1-P9 to efficiently recognize leukemia cells. REVs-Dox/siIDO1-P9 was internalized by leukemia cells to precisely release Dox and siIDO1, resulting in ICD and intracellular IDO1 downregulation, thereby providing a two-pronged antileukemia strategy. Tested in AML allografted mouse models, REVs-Dox/siIDO1-P9 was proved to effectively stimulate DC maturation, activate T cells, and recruit CTLs in the tumor microenvironment, provoking superior antileukemia efficacies and eliciting enhanced immunotherapy.

MATERIALS AND METHODS

Clinical samples

Bone marrow or peripheral blood samples from nine patients with AML were acquired from the First Affiliated Hospital of Chongqing Medical University. The clinical characteristics of the patients are presented in online supplemental table 1.

Cell culture

The AML cell lines (human: THP-1, HL-60; mouse: C1498), human chronic myeloid leukemia (CML) cell line K562 and human bone marrow stromal cell line HS5 were procured from American Tissue Culture Collection (USA). For bioluminescent tracking, THP-1/C1498 cells were transfected with a double-fusion protein reporter containing firefly luciferase (Luc) and green fluorescent protein (GFP), named Luc-GFP-THP-1 and Luc-GFP-C1498. C1498, Luc-GFP-C1498, and HS5 cells were cultured in Dulbecco's Modified Eagle Medium (DMEM) (Gibco, Australia) containing 10% fetal bovine serum (FBS, Gibco), and the rest of the cells were cultured in Roswell Park Memorial Institute (RPMI)-1640 medium (Gibco) containing 10% FBS. AML primary blasts were collected and cultured according to our previous study.[19] The human hematopoietic stem cells (HSCs) were isolated from bone marrow samples of patients with benign hematological diseases (eg, iron

deficiency anemia), using the EasySep human PE Positive/Negative Selection Kit II (STEMCELL) with $CD34^+$ and $CD38^-$ antibodies.

Chemicals

P9 (CDLRSAAVC), P9-PEG_{2k}-DSPE (with/without fluorescein isothiocyanate [FITC] modification), and scramble peptide (Pscr)-PEG_{2k}-DSPE were synthesized by ChinaPeptides. IDO1 siRNA (siIDO1) and cholesterol-conjugated IDO1 siRNA (chol-siIDO1) were synthesized by GenePharma (Shanghai, China). Sequences of siRNAs were as follows: the human siIDO1 (sense strand, 5′-GGGAAGACCCAAAGGAGUUTT-3′), the mouse siIDO1 (sense strand, 5′-GCAAUAUUGCUGUUCC CUATT-3′), the small interfering negative control (siNC) (sense strand, 5′-UUCUCCGAACGUGUCACGUTT-3′), and their Cy5-labeled version were also acquired from GenePharma. Dox was purchased from Sangon Biotech (Shanghai, China). Dialysis bag (MW=12 kDa) was procured from Sigma (USA). 1,1'-Dioctadecyl-3,3,3',3'-Tetramethylindocarbocyanine Perchlorate (DiL), 3,3'-Dioctadecyloxacarbocyanine Perchlorate (DiO), 1,1'-Dioctadecyl-3,3,3',3'-Tetramethylindodicarbocyanine Perchlorate (DiD), and D-luciferin were from Beyotime (Beijing, China), ZFdows Bio (Nanjing, China), Molecular Probes (Eugene, OR, USA) and Maokangbio (Shanghai, China), respectively.

Isolation and purification of REVs

REVs were separated as previously described.[29] Blood samples of blood group O were provided by healthy donors with informed consent. Red blood cells (RBCs) were separated from plasma and white blood cells through centrifugation and leukodepletion filters (Terumo, Japan). Then, RBCs were incubated in phosphate-buffered saline (PBS) containing calcium ionophore (10 µM, Sigma) overnight at 37°C. RBCs and cell debris were removed by sequential centrifugation at 600 × g for 20 min, 1600 × g for 15 min, and 3260 × g for 15 min at 4°C. The supernatant was ultracentrifuged at 100 000 × g for 70 min at 4°C. The sediment was resuspended in PBS and loaded onto a 60% sucrose cushion, followed by ultracentrifugation at 100 000 × g for 16 hours at 4°C. REVs were collected at the interface and washed with PBS at 100 000 × g for 70 min at 4°C. Finally, purified REVs were stored at −80°C. The total protein content and particle concentration of REVs were measured by bicinchoninic acid (BCA) assay and nanoparticle tracking analysis (NTA), respectively. The size distribution and the Zeta potential of REVs were measured with Zetaview (Particle Metrix, Germany), and REVs morphology was observed under transmission electron microscope (TEM). Polydispersity Index was measured with Zetasizer Nano (Malvern, UK). The specific markers of REVs were detected by western blotting. REVs were stained by DiL/DiO/DiD according to the manufacturer's manuals, and the dyed REVs were stored.

Construction and characterization of REVs-Dox/siIDO1-P9

Total 40 µg P9-PEG_{2k}-DSPE was incubated with 100 µL as-prepared REVs for 30 min at 37°C in a shaker to yield P9-functionalized REVs (REVs-P9). Similarly, P9-PEG_{2k}-DSPE (labeled with FITC) was incubated with REVs at 37°C for 0.5 hours, thoroughly washed with PBS, and checked by confocal laser scanning microscopy (CLSM; Leica, Wetzlar, Germany). Then, the fluorescence intensity of purified REVs-P9 was determined with a fluorospectrophotometer (UV2600, Shimadzu, Japan), and the loading efficiency of P9-PEG_{2k}-DSPE was calculated from a quality standard curve.

To entrap Dox into REVs-P9, 40 µg Dox was added to 100 µg REVs-P9 suspended in PBS. The mixture was sonicated in an ice bath at 20% amplitude for six cycles (30 s on, 150 s off) to prepare Dox-loaded REVs (REVs-Dox-P9). After that, it was placed at 37°C for 1 hour to allow REVs membrane recovery. Then the sonicated solution was replaced with RNase-free PBS buffer in preparation for siIDO1 loading. Cholesterol-conjugated siIDO1 (2.5 µg) was added in the PBS buffer with REVs-Dox-P9 (1×10^{10} particles) and shaken at 25°C for 1 hour to form REVs-Dox/siIDO1-P9.[30] Unbound siIDO1 molecules were removed by ultracentrifugation (100 000×g for 70 min at 4°C). The successful loading of siIDO1 was confirmed by a gel retardation assay. Finally, the successfully prepared REVs-Dox/siIDO1-P9 were suspended in PBS for the next study. REVs-Dox/siNC-P9 and REVs-siIDO1-P9 were synthesized as described above.

The amount of Dox loaded into REVs was calculated from a concentration standard curve based on the absorbance intensity at 485 nm using the microplate spectrophotometer (Bio-Tek, USA). For siIDO1 loading capacity, Cy5-labeled siRNA was used, and the fluorescence intensity was evaluated by a fluorospectrophotometer (Shimadzu) and calculated from a concentration standard curve. The siIDO1 number loaded per REVs was calculated by dividing the total retained siIDO1 amount by REVs number.[31] The size distribution, zeta potential, and morphology of REVs-Dox/siIDO1-P9 were measured as mentioned above.

Stability of REVs-Dox/siIDO1-P9

The purified REVs-Dox/siIDO1-P9 were resuspended in PBS (4°C) or serum (37°C) for 7 days. Particle size of REVs-Dox/siIDO1-P9 in PBS or serum was evaluated every day using Zetaview.

In vitro uptake and delivery of REVs

A total of 5×10^5 cells were cultured with DiD-labeled REVs (1×10^6 particles per cell) for 4 hours. The cells were then collected, detecting DiD-positive cells percentage by flow cytometry. To visualize REVs uptake in vitro, approximately 5×10^5 tumor cells were cultured with DiO-labeled REVs (1×10^6 particles per cell) for 4 hours. Subsequently, the cells were washed and fixed with 4% formaldehyde, imaged under CLSM.

In vitro cytotoxicity analysis

The cytotoxicity of REVs (at concentrations of 0 µg/mL, 50 µg/mL, 100 µg/mL, 150 µg/mL, 200 µg/mL, and 300 µg/mL) and the effects of REVs-Dox/siIDO1-P9 (at Dox equiv. 0.2 µg/mL, 0.8 µg/mL, 1 µg/mL, 3 µg/mL, 5 µg/mL, or 10 µg/mL) were determined in HS5, THP-1, HL-60, and C1498 cells using Cell Counting Kit-8 (CCK8; Solarbio, Beijing, China) after incubation for 24 hours. THP-1 and C1498 cells were treated with PBS, free Dox, REVs-Dox/siIDO1-Pscr, and REVs-Dox/siIDO1-P9 (at Dox equiv. 0.2 µg/mL, 0.8 µg/mL, 1 µg/mL, 3 µg/mL, 5 µg/mL, or 10 µg/mL) to detect the cytotoxicity effects of REVs-Dox/siIDO1-P9 by CCK8.

Flow cytometry analysis

For CLL-1 detection, cells were washed twice with cold PBS and stained with anti-CLL-1-FITC (Biolegend, USA) for 30 min at 4°C in the dark, followed by flow cytometry analysis.

Three days post-treatment, bone marrow and draining lymph node samples were collected and dispersed into single cells. Prepared samples were stained with fluorochrome-labeled antibodies. The following antibodies were used: anti-CD11c-APC, anti-CD80-BV421, anti-CD86-PE, anti-CD3-PE, anti-CD8-APC, anti-Ki67-PE, anti-IFN-γ-PE, anti-PD-1-PE, and anti-TIM-3-PE (all from Biolegend).

The Annexin V APC-DAPI staining assay was used for detecting cell apoptosis. THP-1, AML primary blasts, and C1498 cells were treated with free Dox, REVs-Dox/siIDO1-Pscr, and REVs-Dox/siIDO1-P9 (at Dox equiv. 5 µg/mL) for 48 hours. The stained cells were detected using the fluorescence-activated cell sorting (FACS) Calibur instrument (Becton Dickinson, USA).

RNA extraction and quantitative reverse transcription PCR (qRT-PCR)

Total RNA was extracted from cells with Trizol (ThermoFisher, USA). The complementary deoxyribonucleic acid (cDNA) was gained from the purified RNA using a PrimeScript RT Reagent Kit (Takara, Japan). Reverse transcription was performed using 1 µg total RNA and PrimeScript RT Reagent Kit, and then the qRT-PCR reaction was performed with 2 µL cDNA and SYBR Premix Ex Taq II. All experiments were executed at least three times. Primer sequences used are shown in online supplemental table 2.

Western blot analysis

In short, proteins of cells/REVs were extracted with radioimmunoprecipitation assay (RIPA) buffer and quantified by BCA assay kit (Solarbio). After electrophoresis, the protein was transferred to polyvinylidene fluoride (PVDF) membrane, blocked with 5% skim milk, and incubated with primary and secondary antibodies. Blots were detected using an enhanced chemiluminescence (ECL) Kit (MultiSciences, Hangzhou, Zhejiang, China) and visualized by Image Lab. The following antibodies were used according to the manufacturer's manuals: mouse anti-ALG-2-interacting protein X (anti-ALIX) (#sc-53538, Santa Cruz, dilution 1:1,000), rabbit anti-tumor susceptibility gene 101 (anti-TSG101) (#72312, Cell Signaling Technology, dilution 1:1,000), mouse anti-glycophorin A (anti-GPA) (#sc-53905, Santa Cruz, dilution 1: 2,000), rabbit anti-hemoglobin A (anti-HBA) (#sc-21005, Santa Cruz, dilution 1:1,000), mouse anti-ACTIN (#TA-09, ZSGB-BIO dilution 1:1,000), mouse anti-Flotillin-2 (#sc-28320, Santa Cruz, dilution 1:2,000), mouse anti-GM130 (#sc-55590, Santa Cruz, 1:500), mouse anti-calnexin (anti-CANX) (#sc-23954, Santa Cruz, dilution 1:500), rabbit anti-glyceraldehyde-3-phosphate dehydrogenase (anti-GAPDH) (#sc-25778, Santa Cruz, dilution 1:1,000) and mouse anti-Stomatin (anti-STOM) (#sc-376869, Santa Cruz, dilution 1:1,000).

Confirmation of ICD

After 24 hours Dox or REVs-Dox/siIDO1-P9 treatment, cell culture supernatant of THP-1 and leukemia primary blasts was collected and measured using the ATP Assay Kit (Solarbio) and the Human HMGB1 ELISA Kit (Elabscience, Wuhan, China). Meanwhile, the cells were fixed with 4% paraformaldehyde. Then, cells were incubated overnight with rabbit anti-CRT (#27 298–1-AP, Proteintech, dilution 1:50) or rabbit anti-HMGB1 (#A5052, Selleck, dilution 1:50) antibody at 4°C, and incubated with secondary antibody for 1 hour at 25°C. Subsequently, stained with DAPI, the cells were imaged using CLSM. To evaluate the ICD effects in vivo, we subcutaneously injected 1×10^6 C1498 cells into C57BL/6 mice. The mice were given PBS, free Dox, and REVs-Dox/siIDO1-P9 (3 mg/kg Dox equivalent) intravenously when the tumor volume reached 100 mm^3. After 48 hours, the tumors were collected, and interstitial fluid was acquired by centrifuging. ATP and HMGB1 release were detected as mentioned above.

In vitro induction of DC maturation

Human peripheral blood mononuclear cells (PBMCs)-derived DCs were prepared according to a previous study.[32] Briefly, human monocytes were acquired by plastic adherence of PBMCs. The enriched monocytes were placed in medium containing 100 ng/mL human granulocyte-macrophage colony-stimulating factor (GM-CSF, PeproTech, America) and 20 ng/mL human interleukin (IL) 4 (InvivoGen, France) for 2 days. Subsequently, the medium was changed, and 10 ng/mL tumor necrosis factor-alpha (TNF-α, InvivoGen) was added for 24 hours to obtain human DCs. Treated with PBS/Dox/REVs-Dox/siIDO1-P9 (at Dox equivalent 5 µg/mL) for 12 hours, AML primary blasts were washed and co-cultured with human DCs for another 12 hours. The maturation of DCs ($CD80^+CD86^+$) was detected with flow cytometry.

AML animal models establishment

To generate AML-xenografted mice, Luc-GFP-THP-1 cells (1×10^6, PBS suspension) were intravenously

injected into NOD-Prkdc^{scid} Il2rg^{null} (NCG) mouse (female, 6–8 weeks, GemPharmatech). To generate AML-allografted mice, C57BL/6 mice (female, 6–8 weeks, the laboratory animal center of Chongqing Medical University) were injected intravenously with 5×10^5 Luc-GFP-C1498 cells. To confirm the onset of leukemia, the mice were intraperitoneally injected with D-luciferin (150 µg/g) to monitor leukemia signals via bioluminescent imaging with the In Vivo Imaging System (the Berthold Technologies LB983). When the bioluminescence signal became visible, it indicated that the AML animal model was successfully generated. Prior to treatment initiation, mice were stratified based on quantitative bioluminescence imaging signal intensity to ensure equivalent leukemia burden across groups. Mice with comparable leukemia burden were then randomly allocated into treatment groups.

In vivo uptake and delivery of REVs-Dox/siIDO1-P9

To detect REVs uptake by leukemia cells (GFP$^+$) in vivo, leukemia mice were injected intravenously with REVs-Dox/siIDO1-Pscr or REVs-Dox/siIDO1-P9 (labeled with DiD, 3×10^{10} particles/injection). After 6 hours, mice were euthanized and tissues (bone marrow, liver, spleen, and peripheral blood) were obtained. Subsequently, the single-cell suspension is prepared as described above. DiD$^+$GFP$^+$ fluorescence signal was measured through flow cytometry.

In vivo antileukemia activity of REVs-Dox/siIDO1-P9

The anti-leukemogenic effect of REVs-Dox/siIDO1-P9 was observed in C57BL/6 mice. Successfully allografted mice were randomized into five groups and intravenously injected with PBS, REVs, REVs-Dox/siNC-P9, REVs-siIDO1-P9, or REVs-Dox/siIDO1-P9 (3×10^{10} particles for each dose: Dox equivalent 3 mg/kg and siIDO1 equivalent 5 nmol/kg) every 2 days for a total of six times. Body weights were monitored during treatment progress at regular intervals. Three days post-treatment, bioluminescent imaging was performed. Subsequently, the mice were euthanized, and the spleens were weighed. Bone marrow cells were isolated and stained with Giemsa. The spleens, livers, and lungs were harvested for H&E staining. Additionally, the percentage of GFP$^+$ AML cells was detected by flow cytometry. Kaplan-Meier survival analysis was conducted in another batch.

In vivo biosafety of REVs-Dox/siIDO1-P9

To assess in vivo biosafety of REVs-Dox/siIDO1-P9, C57BL/6 mice were treated six times with PBS, REVs, and REVs-Dox/siIDO1-P9 (3×10^{10} particles/injection), respectively. The day after the last injection, blood samples were drawn for routine hematological and biochemical tests. The main tissues (spleen, liver, heart, lung, and kidney) were harvested for H&E staining. Body weight change after treatment was monitored in another batch of experiments at regular intervals.

Statistical analysis

All the data were analyzed by GraphPad Prism V.7.0 software and presented as means±SD. Comparisons between two groups were performed using Student's t-test, and multiple groups were compared using analysis of variance (ANOVA). Statistical significance was defined as *p<0.05, **p<0.01, ***p<0.001.

RESULTS

Construction of REVs-Dox/siIDO1-P9

The steps to construct the REVs-based multifunctional co-delivery nanosystems are outlined in online supplemental scheme 1. First, REVs derived from RBCs of blood group O were purified by sequential ultracentrifugation processes. The purified REVs were characterized following the International Society for Extracellular Vesicles recommendations.[33] REVs were enriched in extracellular vesicle (EV) markers (ALIX, TSG101), RBC lipid raft-associated membrane proteins (Flotillin-2, STOM), and RBC-specific proteins (HBA). Also, REVs expressed GPA, an exclusive marker for EVs originated from human RBCs, but completely lacked CANX (an endoplasmic reticulum marker) and GM130 (Golgi apparatus markers). The cytoskeleton protein β-actin was largely absent in REVs, suggesting the effective removal of cellular fragments during purification (figure 1A). Checked by TEM and NTA, REVs were cup-shaped vesicles with an average diameter of ~156.7 nm (figure 1B,C) and a Polydispersity Index ~0.06 (figure 1D). These REVs were negatively charged with a Zeta potential of −9.89 mV (figure 1E). To procure P9-modified REVs (REVs-P9), P9 peptide was initially linked with DSPE-PEG$_{2k}$-NHS (N-Hydroxysuccinimide) to obtain P9-PEG$_{2k}$-DSPE (online supplemental figure 1A), which can spontaneously insert into REVs membrane.[34] By confocal microscope, 75.7% of REVs (labeled with DiL) co-localized with P9-PEG$_{2k}$-DSPE (labeled with FITC) (online supplemental figure 1B), and the P9 loading efficiency was 56.1% (online supplemental figure 1C).

For REVs-Dox-P9 preparation, Dox was sonicated into REVs-P9, followed by ultracentrifugation to collect the pellet. Dox loading efficiency was measured to be 32.01% based on the standard curve (online supplemental figure 1D). To verify Dox encapsulation in REVs, we dialyzed the ultracentrifugation pellet to remove unentrapped Dox (1 hour, cut-off: 12 kDa).[35 36] Re-quantification of Dox loading efficiency postdialysis revealed no significant change compared with predialysis levels (online supplemental figure 1D), confirming successful encapsulation of Dox within REVs rather than non-specific aggregation. Notably, no significant differences were observed in vesicle morphology (shape and intact membranes) or particle size distribution presonication and postsonication (average diameter: ~167 nm, online supplemental figure 1E). Next, we anchored siIDO1 with a 5'-tetra (ethylene glycol) spacer and cholesterol modification (chol-siIDO1) to REVs-Dox-P9 by co-incubation. As

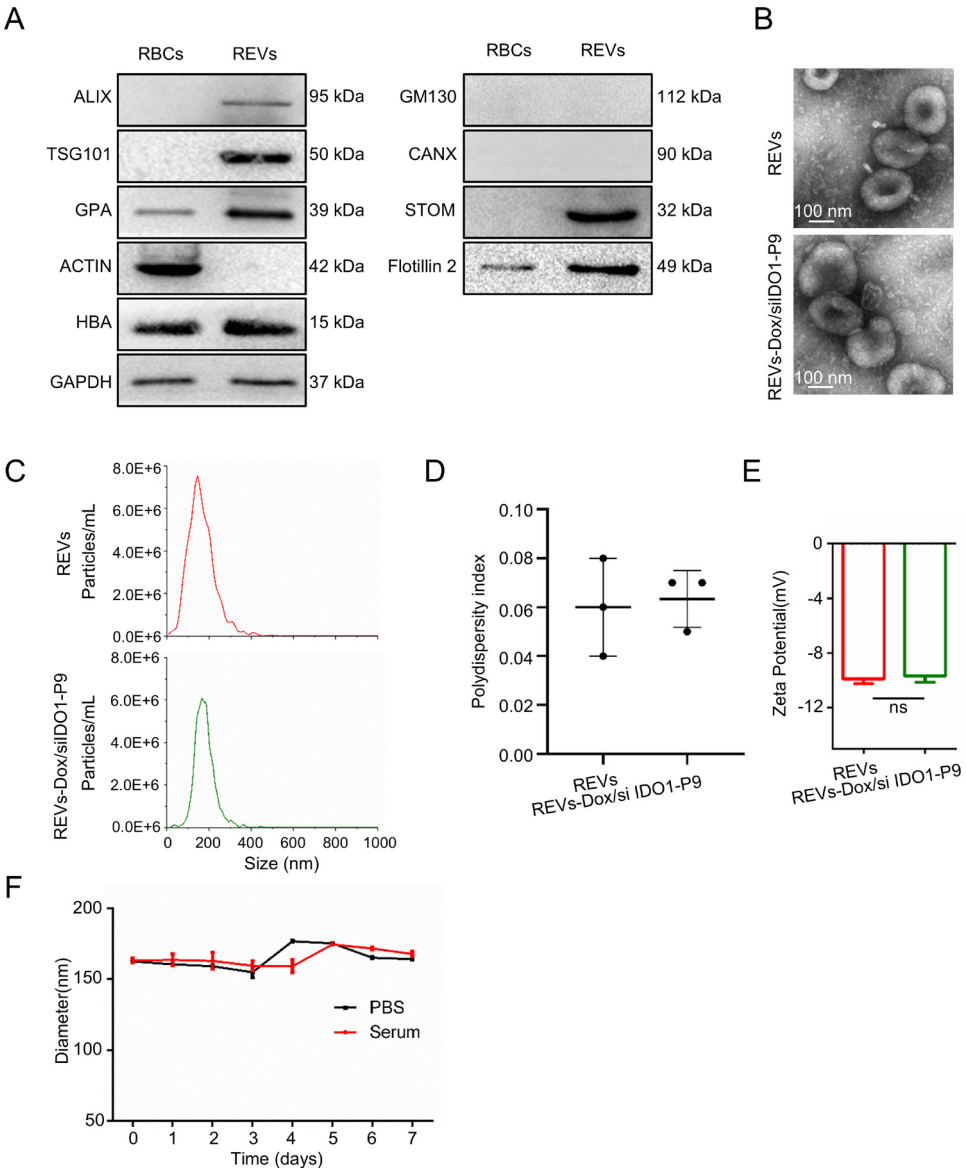

Figure 1 Construction and characterization of REVs-Dox/siIDO1-P9. (A) Characterization of RBCs and REVs' protein content by Western blotting. (B) Representative TEM images of REVs and REVs-Dox/siIDO1-P9. (C) Size distribution of REVs and REVs-Dox/siIDO1-P9. (D) Polydispersity Index of REVs and REVs-Dox/siIDO1-P9. (E) The Zeta potential of REVs and REVs-Dox/siIDO1-P9. (F) Stability of REVs-Dox/siIDO1-P9. Particle size by Zetaview of REVs-Dox/siIDO1-P9 incubated in PBS or serum for indicated days. Data were presented as mean±SD (n=3 independent experiments). Student's t-test in E. CANX, calnexin; STOM, stomatin; Dox, doxorubicin; GPA, glycophorin A; HBA, hemoglobin A; IDO1, indoleamine 2,3-dioxygenase-1; ns, not significant; REVs, red blood cell-derived extracellular vesicles; TEM, transmission electron microscope.

shown in online supplemental figure 1F, the green fluorescence spots of DiO-REVs and red fluorescence spots of Cy5-siIDO1 were effectually overlapping, with an average diameter of ~162.2 nm, suggesting the successful loading of siRNA in REVs. To prove the successful loading of siIDO1, we performed a gel retardation assay comparing preultracentrifugation complexes with postultracentrifugation complexes. Our results demonstrated that unloaded siRNA was detected at the bottom of the agarose gel in the preultracentrifugation complexes, whereas the postultracentrifugation complexes exhibited siRNA retention in the wells (online supplemental figure 1G), suggesting effective siRNA loading onto REVs. According to the standard curve of Cy5-siIDO1, siRNA loading efficiency was approximately 19.84% (online supplemental figure 1H), and approximately 2054 molecules of Cy5-siIDO1 were loaded into per REVs (online supplemental figure 1I). These data demonstrated that the engineered REVs (REVs-Dox/siIDO1-P9) with required functional molecules and therapeutic agents were successfully constructed.

Next, we explored whether REVs-Dox/siIDO1-P9 could maintain the typical REVs properties after modification. Similar to the empty REVs, REVs-Dox/siIDO1-P9 was also negatively charged (−9.69 mV) and displayed similar and intact morphology (figure 1B and E), whereas the

diameter of REVs-Dox/siIDO1-P9 was increased to ~171 nm (figure 1C). These results indicated that the process to obtain REVs-Dox/siIDO1-P9 didn't appreciably change the physicochemical property of REVs. Given that serum stability is a key factor for the drug delivery platform, REVs-Dox/siIDO1-P9 was then suspended in PBS and serum over 7 days. REVs-Dox/siIDO1-P9 had no obvious size change (figure 1F), unveiling their high application stability.

REVs-Dox/siIDO1-P9 is taken up efficiently by leukemia cells in vitro

Efficient internalization by recipient cells is the prerequisite for the biosystem to exert their effects. We initially assessed CLL-1 surface expression across AML cell lines (THP-1, HL-60, and C1498) and AML primary blasts. Flow cytometric analysis revealed consistently detectable CLL-1 expression levels in AML cells (online supplemental figure 2A). Notably, primary AML specimens exhibited CLL-1 expression with varying signal intensities (online supplemental figure 2B). This expression pattern was observed across multiple French-American-British (FAB) subtypes (online supplemental table 1), demonstrating its prevalence in diverse AML classifications. However, bone marrow stromal cells (HS5) showed virtually no expression of CLL-1 (online supplemental figure 2A). Most importantly, HSCs ($CD34^+CD38^-$) lacked the CLL-1 expression (online supplemental figure 2C). Leukemia cells were incubated with engineered REVs for 4 hours, and phagocytosis efficiency of the delivery biosystem was monitored by flow cytometry. REVs-Dox/siIDO1-P9, rather than scrambled P9 (Pscr)-ligated-REVs (REVs-Dox/siIDO1-Pscr), was highly internalized by THP-1, C1498 cells, and AML primary blasts (figure 2A). However, both HSCs and HS5 cells exhibited minimal uptake of REVs-Dox/siIDO1-P9 and REVs-Dox/siIDO1-Pscr (online supplemental figure 3A). Similarly, CLSM images showed the P9 peptide markedly improved the uptake of DiO-labeled REVs by CLL-1-positive AML cells, such as THP-1, C1498 cells, and AML primary blasts, but not the CLL-1-negative K562 cells (figure 2B, online supplemental figures 2A and 3B,C),[37] indicating our biosystem can effectively and specifically target CLL-1-positive AML cells. To further confirm whether the REVs uptake by CLL-1-positive AML cells needs the specific interaction of P9 and CLL-1, THP-1, C1498 cells, and AML primary blasts were pretreated with free P9 peptide. As expected, pretreatment of leukemia cells with free P9 peptide obviously impaired the P9-mediated REVs uptake (figure 2B, online supplemental figure 3B,C). Taken together, these data demonstrated that the P9-modified REVs could be efficiently taken up by CLL-1-positive leukemia cells in vitro.

Next, cytotoxicity and killing effect of REVs-Dox/siIDO1-P9 were evaluated. HS5 cells are an immortalized human bone marrow stromal cell line, which is widely used as an "in vitro" model to study drug responses. To assess cytotoxicity, HS5 cells and leukemia cells (THP-1, HL-60, and C1498) were treated with REVs and REVs-Dox/siIDO1-P9 in a dose-dependent manner. We found that HS5 and all experimental leukemia cells were not obviously affected by REVs under low or high concentrations treatment (online supplemental figure 3D). However, compared with leukemia cells, REVs-Dox/siIDO1-P9 provided less toxicity to HS5 cells (online supplemental figure 3E), suggesting that the delivery carrier was non-cytotoxic to cells and REVs-Dox/siIDO1-P9 mitigated toxicity to the marrow stromal cells. To further evaluate REVs-Dox/siIDO1-P9's toxicity, HS5 cells and HSCs ($CD34^+CD38^-$) were treated with equivalent doses of free Dox and REV-Dox/siIDO1-P9. As shown in online supplemental figure 3F–I, compared with free Dox, REV-Dox/siIDO1-P9 showed significantly reduced toxicity towards HS5 cells and HSCs. Then, we evaluated the killing efficiency of REVs-Dox/siIDO1-P9 to leukemia cells. About 17% of THP-1 and 35% of C1498 cells kept in survival under REVs-Dox/siIDO1-P9 treatment (5 µg/mL) for 24 hours, which is comparable with free Dox (at the same concentration) in the killing effect (figure 2C). Of note, compared with REVs-Dox/siIDO1-P9, the leukemia cell-killing effect of REVs-Dox/siIDO1-Pscr was lower, possibly due to the poor targeting selectivity of REVs-Dox/siIDO1-Pscr (figure 2C). In addition, the total apoptotic rate in leukemia cells treated with REVs-Dox/siIDO1-P9 was also significantly higher than that of REVs-Dox/siIDO1-Pscr (figure 2D, online supplemental figure 3J). Finally, the gene transfection ability of the biosystem was assessed. Both REVs-Dox/siIDO1-Pscr and REVs-Dox/siIDO1-P9 could suppress the expression level of IDO1 in THP-1 cells, C1498 cells, and AML primary blasts, whereas REVs-Dox/siIDO1-P9 treatment showed higher efficacy (figure 2E–G). Taken together, the REVs-based biosystem was efficiently delivered to leukemia cells and performed its functions well in vitro.

REVs-Dox/siIDO1-P9 is effectively delivered to leukemia cells in vivo

Based on in vitro uptake results, the tumor-targeting ability of REVs-Dox/siIDO1-P9 was examined in vivo. To generate AML-xenografted and allografted mice, Luc-GFP-THP-1 and Luc-GFP-C1498 cells were injected intravenously into NCG and C57BL/6 mice, respectively. When leukemic bioluminescent signals became apparent and accumulated highly, DiD-labeled REVs-Dox/siIDO1-Pscr and REVs-Dox/siIDO1-P9 were injected into leukemia-bearing mice. The accumulation of DiD^+ REVs in GFP^+ leukemia cells was examined (figure 3A). As expected, P9 conjugation increased the percentage of DiD^+ THP-1 cells from 29.0% to 68.3% in bone marrow, and from 29.3% to 64.2% in peripheral blood (figure 3B). In addition, REVs uptake in the spleen and liver was also increased with the presence of P9 (figure 3B). Similar results of REVs uptake were also detected in AML-allografted mice (online supplemental figure 4A,B). Next, we investigated whether REVs-Dox/siIDO1-P9 could effectively deliver siIDO1 into leukemia cells and exert its knockdown function in

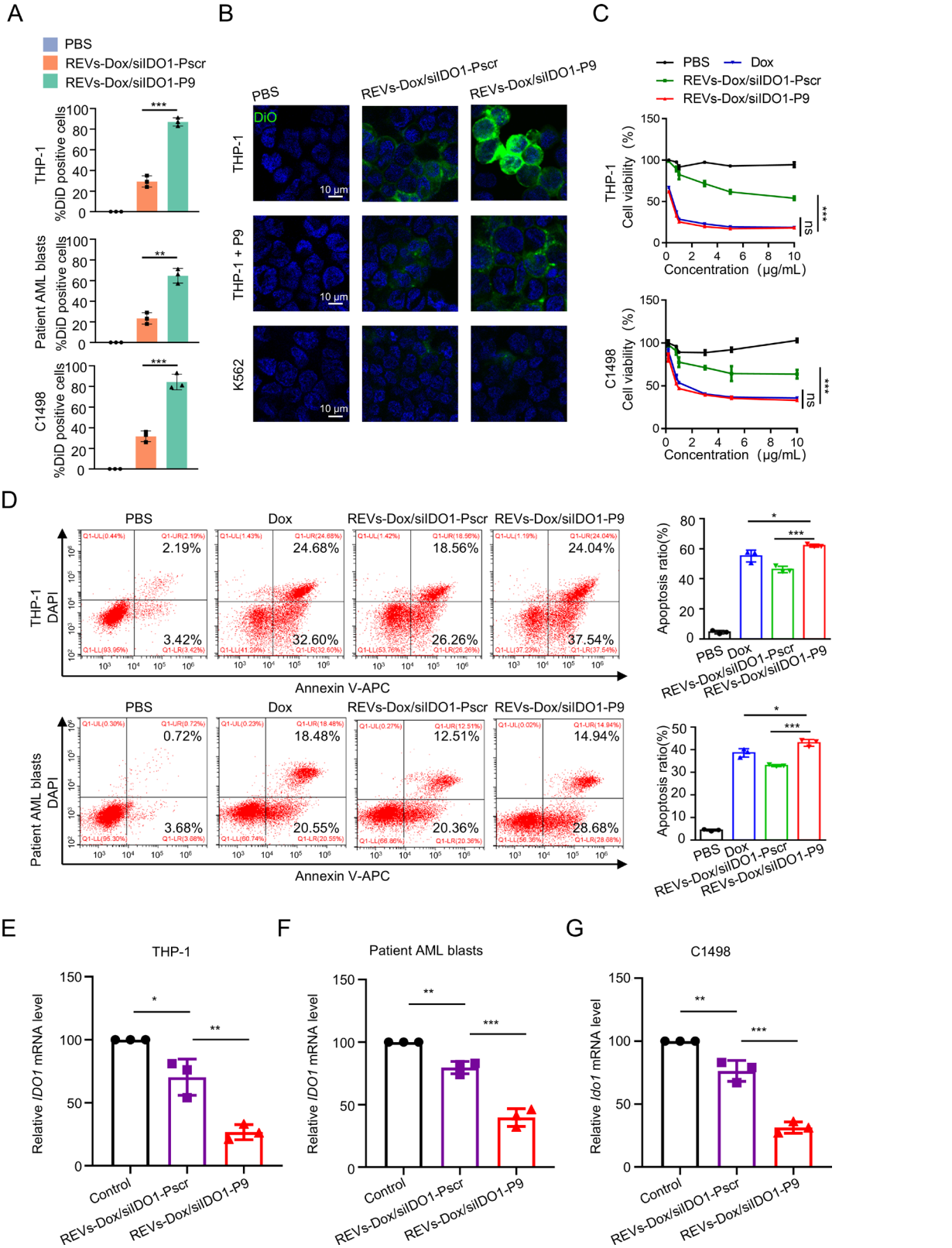

Figure 2 REVs-Dox/siIDO1-P9 is taken up efficiently by leukemia cells in vitro. (A) Percentage of DiD-positive THP-1/patient AML blasts/C1498 cells. (B) CLSM images showing the cellular uptake of REVs in THP-1/K562 cells. (C) Viability of THP-1 and C1498 cells in the indicated groups. (D) Apoptosis analysis of THP-1 cells and patient AML blasts treated with PBS/Dox/REVs-Dox/siIDO1-Pscr/REVs-Dox/siIDO1-P9. Right, statistical analysis. (E–G) Relative IDO1 mRNA levels in THP-1 cells (E), patient AML blasts, (F) and C1498 cells (G). Data were presented as mean±SD (n=3 independent experiments). One-way ANOVA test in A, D, E, F, and G; two-way ANOVA test in C. *p<0.05; **p<0.01; ***p<0.001; AML, acute myeloid leukemia; ANOVA, analysis of variance; CLSM, confocal laser scanning microscopy; Dox, doxorubicin; IDO1, indoleamine 2,3-dioxygenase-1; Pscr, scramble peptide; REVs, red blood cell-derived extracellular vesicles.

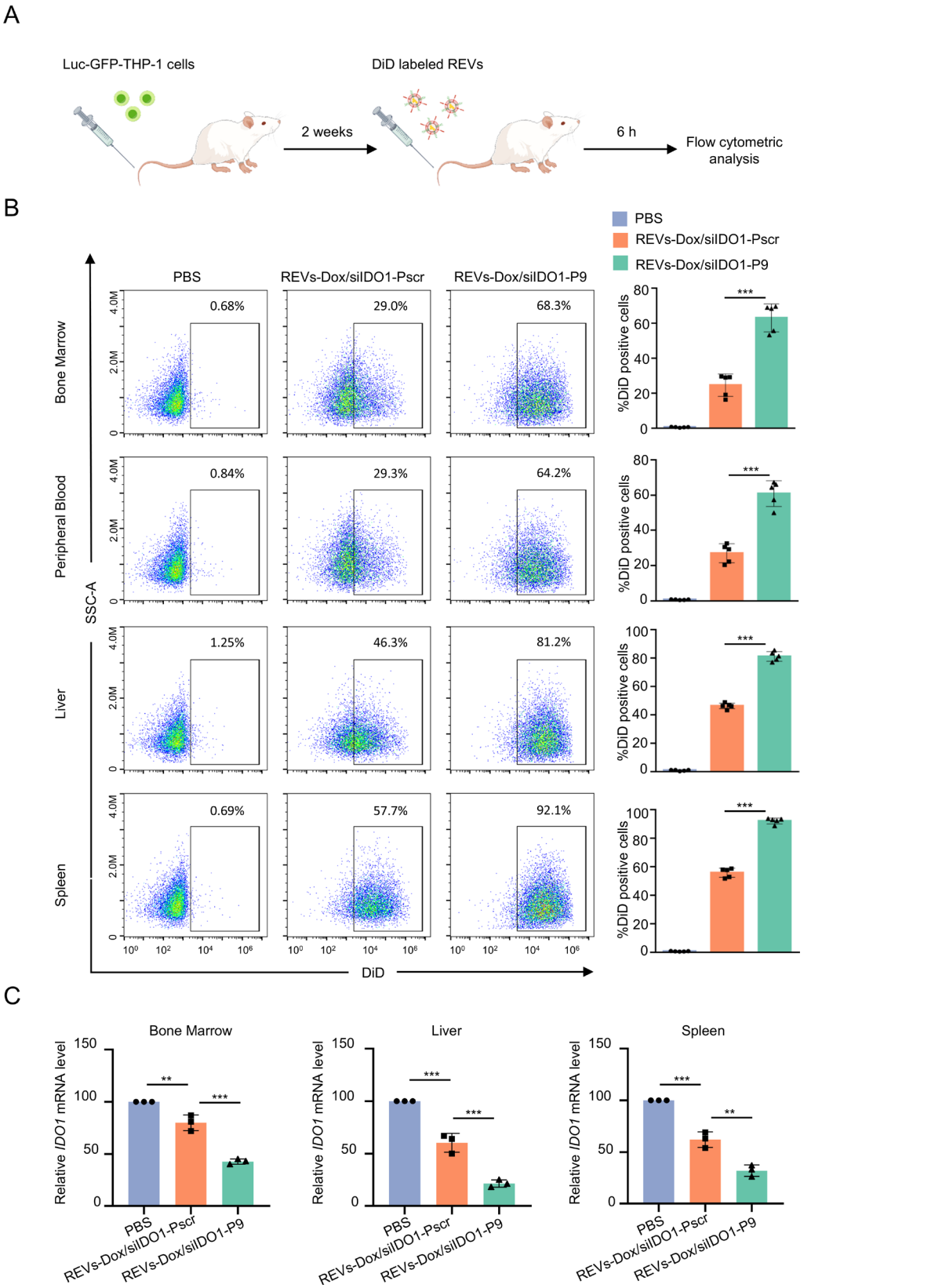

Figure 3 REVs-Dox/siIDO1-P9 is effectively delivered to leukemia cells in vivo. (A) Workflow for determination of REVs-Dox/siIDO1-P9 uptake in AML-xenografted mice. (B) Left, flow cytometric analysis manifesting the uptake of DiD-labeled REVs by GFP$^+$ THP-1 cells, gated based on DiD expression, in bone marrow, peripheral blood, liver, and spleen. Right, statistical analysis (n=5 mice per group). (C) Relative IDO1 mRNA levels of THP-1 cells in bone marrow, liver, and spleen. Data were presented as mean±SD (n=3 independent experiments). One-way ANOVA test in B and C. **p<0.01; ***p<0.001. SSC-A, side scatter area; ANOVA, analysis of variance; Dox, doxorubicin; GFP, green fluorescent protein; IDO1, indoleamine 2,3-dioxygenase-1; Luc, luciferase; Pscr, scramble peptide; REVs, red blood cell-derived extracellular vesicles.

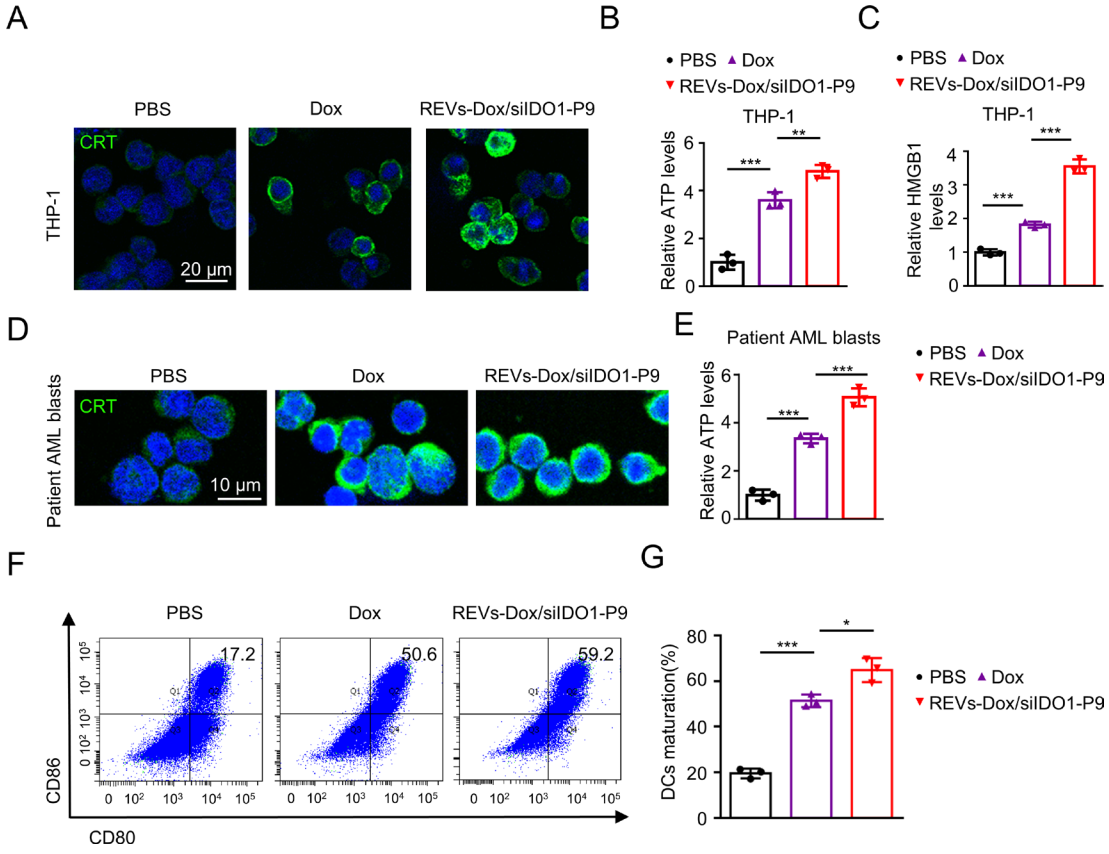

Figure 4 ICD induction effect of REVs-Dox/siIDO1-P9**.** (A and D) CLSM images of the surface exposure of CRT on THP-1 cells (A) and primary leukemia cells (D) in the indicated groups. (B–C) Extracellular ATP levels (B) and HMGB1 release levels (C) of THP-1 cells. (E) Extracellular ATP levels in primary leukemia cells. (F) DCs maturation ($CD80^+CD86^+$) was evaluated by flow cytometry (gated on $CD11c^+$ cells). (G) Quantitative analysis of the data shown in panel (F). Data were presented as mean±SD (n=3 independent experiments). One-way ANOVA test in B, C, E, and G. *p<0.05; **p<0.01; ***p<0.001. AML, acute myeloid leukemia; ANOVA, analysis of variance; CD11c, cluster of differentiation 11 c; CD80, cluster of differentiation 80; CD86, cluster of differentiation 86; CLSM, confocal laser scanning microscopy; CRT, calreticulin; DCs, dendritic cells; Dox, doxorubicin; HMGB1, high mobility group box 1; ICD, immunogenic cell death; IDO1, indoleamine 2,3-dioxygenase-1; REVs, red blood cell-derived extracellular vesicle.

vivo by qRT-PCR. As expected, IDO1 expression levels were notably decreased in leukemia cells isolated from bone marrow, liver, and spleen in both AML-xenografted and allografted mice after 24 hours treatment (figure 3C; online supplemental figure 4C). Therefore, REVs-Dox/siIDO1-P9 can be efficiently delivered into leukemia cells and function well in vivo.

ICD induction effect of REVs-Dox/siIDO1-P9

Previous reports suggested that ICD triggers tumor cells to release immunogenic DAMPs such as CRT, ATP, and HMGB1.[38 39] ICD cascade can induce DC maturation and recruit activated CTLs in the tumor microenvironment.[40] Whether REVs-Dox/siIDO1-P9 could induce ICD was investigated. Under REVs-Dox/siIDO1-P9 treatment, THP-1 cells showed elevated CRT exposure on the cell surface (figure 4A) and enhanced ATP and HMGB1 release (figure 4B,C). Compared with free Dox treatment, REVs-Dox/siIDO1-P9 treated THP-1 cells exhibited a stronger CRT exposure and a higher ATP and HMGB1 release, due to the fact that REVs-Dox/siIDO1-P9 could effectively deliver the cargo into leukemia cells in vitro. Consistently, CRT exposure, ATP release, and HMGB1 secretion of patient AML blasts were significantly increased in the REVs-Dox/siIDO1-P9 group (figure 4D,E; online supplemental figure 5A). REVs-Dox/siIDO1-P9 treatment was also found to facilitate C1498 cells to release more ATP and HMGB1 in vivo (online supplemental figure 5B,C). Furthermore, AML primary blasts treated with REVs-Dox/siIDO1-P9 increased the percentage of mature DCs (59.2%) in vitro in contrast with free Dox induction (50.6%, figure 4F,G). Collectively, REVs-Dox/siIDO1-P9 could induce ICD in leukemia cells.

In vivo antitumor efficacy of REVs-Dox/siIDO1-P9

Based on the above results, we tried to evaluate the potential therapeutic efficacy of REVs-Dox/siIDO1-P9 in vivo. C57BL/6 mice with comparable leukemia burden were randomly allocated into five groups and treated with PBS, REVs, REVs-Dox/siNC-P9, REVs-siIDO1-P9, and REVs-Dox/siIDO1-P9 via tail vein injection (figure 5A, online supplemental figure 6A). Leukemia burden was monitored using bioluminescent imaging. As shown in figure 5B, leukemic bioluminescent signals of mice

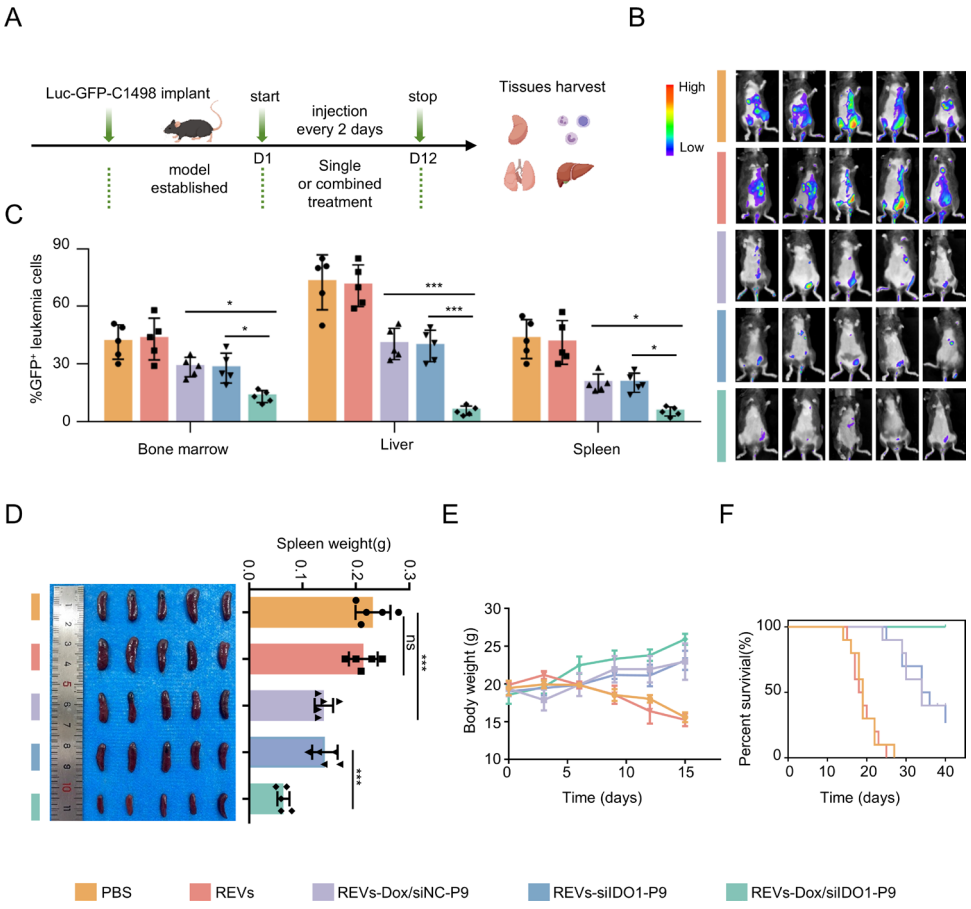

Figure 5 In vivo antitumor efficacy of REVs-Dox/siIDO1-P9. (A) Schematic schedule for targeted chemo-immunotherapy in C1498 leukemia-bearing mice via intravenous injection. (B) Luminescence images of mice after various treatments. (C) Percentage of GFP$^+$ C1498 cells in bone marrow, liver, and spleen from the indicated groups. (D) Representative external views and weights of spleens from mice received different treatments. (E) Body weight change of AML mice during treatment. (F) Survival curves for indicated groups (n=10 mice per group). Data were presented as mean±SD (n=5 mice per group, unless noted). One-way ANOVA test in C and D. *p<0.05; ***p<0.001; ANOVA, analysis of variance; Dox, doxorubicin; GFP, green fluorescent protein; IDO1, indoleamine 2,3-dioxygenase-1; Luc, luciferase; ns, not significant; REVs, red blood cell-derived extracellular vesicles.

treated with PBS and empty REVs were widely distributed, prominently in the bone marrow, liver, and spleen. Compared with the mice treated by PBS and empty REVs, the mice injected with REVs-Dox/siNC-P9 or REVs-siIDO1-P9 had obviously reduced leukemic burden (figure 5B). Importantly, the mice treated with REVs-Dox/siIDO1-P9 exhibited a synergistic therapy effect, appearing to have the lowest leukemic bioluminescent signal (figure 5B). REVs-Dox/siIDO1-P9 treated mice had the least percentage of GFP$^+$ C1498 cells in the bone marrow, liver, and spleen in comparison with mice treated with REVs-Dox/siNC-P9 or REVs-siIDO1-P9 (figure 5C). In accordance with these results, REVs-Dox/siIDO1-P9 treatment conspicuously reduced the signs of leukemic cells in bone marrow, which were accompanied by a decrease in dense clusters of morphologically immature granulocytes, checked by morphological analysis of bone marrow cells (online supplemental figure 6B). Splenomegaly, a hallmark of extramedullary hematopoiesis in AML,[41] was markedly alleviated after REVs-Dox/siIDO1-P9 treatment, evidenced by reduced spleen size and weight (figure 5D). In contrast, the mice injected with PBS or single agent had enlarged spleens with a certain degree of damage to the red and white pulp (figure 5D and online supplemental figure 6C). REVs-Dox/siIDO1-P9 treated mice showed the most significant improvement in extramedullary infiltration, validated by a decrease in the area of liver infiltration and the number of lung metastatic nodules (online supplemental figure 6D,E). In addition, leukemia-bearing mice who received REVs-Dox/siIDO1-P9 treatment had no or less weight loss, with a significantly extended lifespan (figure 5E,F). In conclusion, REVs-Dox/siIDO1-P9 exerts excellent AML-suppressive efficacy in vivo.

REVs-Dox/siIDO1-P9 promotes in vivo immune activation

Next, whether REVs-Dox/siIDO1-P9 treatment would facilitate immune activation in AML allografted mice was determined. DCs play a crucial role in promoting immune response in tumor-draining lymph nodes and CD8$^+$ CTL infiltration.[42] The draining lymph nodes of mice (subjected to PBS, REVs, REVs-Dox/siNC-P9,

REVs-siIDO1-P9, and REVs-Dox/siIDO1-P9 treatments) were collected for DC maturation analysis. Compared with the PBS or REVs group, Dox-loaded REVs (REVs-Dox/siNC-P9) could increase the number of mature DCs to 20.5% (figure 6A), and REVs-Dox/siIDO1-P9 effectively increased DC maturation to approximately 23.2% (figure 6A), indicating that the dual delivery biosystem can synergistically promote DC maturation in vivo. Consistently, treatment with REVs-Dox/siIDO1-P9 resulted in the highest ratio of $CD8^+$ T cells (15.2%), which shows chemoimmunological cascade therapy could effectively facilitate $CD8^+$ T cell infiltration in the bone marrow (figure 6B). Concurrently, the administration of REVs-Dox/siIDO1-P9 significantly increased the activation and proliferation of tumor-infiltrating $CD8^+$ T cells (figure 6C,D). These findings demonstrated that REVs-Dox/siIDO1-P9 treatment could provide more comprehensive T cell activation benefits compared with single delivery systems. We then explored $CD8^+$ T cell exhaustion following REVs-Dox/siIDO1-P9 treatment. Since the enhanced programmed cell death-1 (PD-1) and T cell immunoglobulin-containing and mucin-domain-containing-3 (TIM-3) work as key indicators of $CD8^+$ T cell exhaustion,[43 44] we thus compared PD-1 and TIM-3 levels of $CD8^+$ T cells from mice subjected to PBS, REVs, REVs-Dox/siNC-P9, REVs-siIDO1-P9, and REVs-Dox/siIDO1-P9 treatments. The siIDO1-loaded REVs (REVs-siIDO1-P9) remarkably decreased the percentage of $PD\text{-}1^+$ and $TIM\text{-}3^+$ $CD8^+$ T cells, indicating a reduction in T cell exhaustion with siIDO1 intervention (figure 6E,F). REVs-Dox/siIDO1-P9 treatment further reduced the proportion of exhausted $CD8^+$ T cells (figure 6E,F). Overall, these data confirmed that REVs-Dox/siIDO1-P9 has a stronger advantage than REVs-Dox/siNC-P9 and REVs-siIDO1-P9 in promoting immune activation in vivo.

Biosafety assessment of REVs-Dox/siIDO1-P9 in vivo

The remarkable antileukemia effect of REVs-Dox/siIDO1-P9 observed in vivo warrants further investigation into their biosafety for potential application in AML therapy. Evaluation initially focused on potential biological toxicity to major organs (spleen, liver, heart, lung, and kidney) using H&E staining of tissue sections (figure 7A). No signs of organ inflammation or injury were detected across treatment groups. Hematological parameters (WBC,white blood cell; RBC, red blood cell; HGB, hemoglobin; HCT, hematocrit; MCV, mean corpuscular volume; MCH, mean corpuscular hemoglobin; MCHC, mean corpuscular hemoglobin concentration; PLT, platelet) and blood biochemical markers (ALT, alanine aminotransferase; AST, aspartate aminotransferase; DBIL, direct bilirubin; ALP, alkaline phosphatase; BUN, blood urea nitrogen; CK, creatine kinase) kept in normal ranges, displaying a favorable safety profile (figure 7B,C). Moreover, the mice treated with REVs or REVs-Dox/siIDO1-P9 showed a consistent and stable increase in body weight as the mice treated by vehicle (online supplemental figure 7). Thus, our study provides strong data to support that REVs-Dox/siIDO1-P9 may be promising and safe for application in AML therapy.

DISCUSSION

AML remains one of the most lethal hematological malignancies. This underscores the critical need for developing innovative and tailored treatments for the disease. In the present study, we established AML-targeting REVs that encapsulated functional siIDO1 and Dox, which activated DCs, induced $CD8^+$ T cell infiltration, and relieved the exhaustion state of $CD8^+$ T cells, thereby enhancing therapeutic outcomes in AML.

The failure of phase III clinical trials with small-molecule IDO1 inhibitors like epacadostat highlights significant challenges in translating Trp pathway biology into successful cancer treatments.[45] Various factors have been suggested for these negative results, including the absence of patient preselection based on IDO1 expression, inadequate IDO1 inhibition, and epacadostat's off-target effects.[45] A novel approach involves combining IDO1 inhibition with established therapies, which in our study activated the tumor microenvironment by increasing immune cell infiltration. This shift towards a more immunostimulatory tumor microenvironment enhanced antitumor immunity, resulting in enhanced tumor suppression and prolonged survival in mouse models. Proof-of-concept experiments demonstrated that epacadostat in combination with chemotherapy could effectively alleviate recurrent relapses in patients with AML receiving chemotherapy, supporting our findings.[7]

Most current tumor immunotherapy strategies heavily rely on the presence of tumor-infiltrating lymphocytes within the tumor microenvironment. Nevertheless, challenges such as the complicated tumor microenvironment composition, immunosuppressive environment, and low immunogenicity of certain tumors hinder achieving optimal clinical outcomes.[46–50] In other words, host immune responses are often insufficient in an immunocompromised context, potentially accounting for the greater efficacy of combination therapy over monotherapy in our study. Effective combinations of chemotherapy and immunotherapy can address issues related to clonal evolution and therapy-resistant clones, promoting durable remission in AML. Additionally, the positive effects of chemo-immunotherapy have been observed in various other tumors.[51 52]

Tryptophan catabolism plays an important role in leukemic cells.[53–57] Kyn levels increased in patients with AML. However, whether Kyn acts as a biomarker or active determinant of disease progression remains unknown, which needs to be explored in future work. Targeting Kyn combined with chemotherapy may display more immediate effects.

Ensuring clinical translation involves maintaining biosafety and reproducibility in drug delivery systems. EVs, owing to their biocompatibility and stability, offer advantages over traditional synthetic delivery systems. REVs, known for their abundance, scalability, and absence of

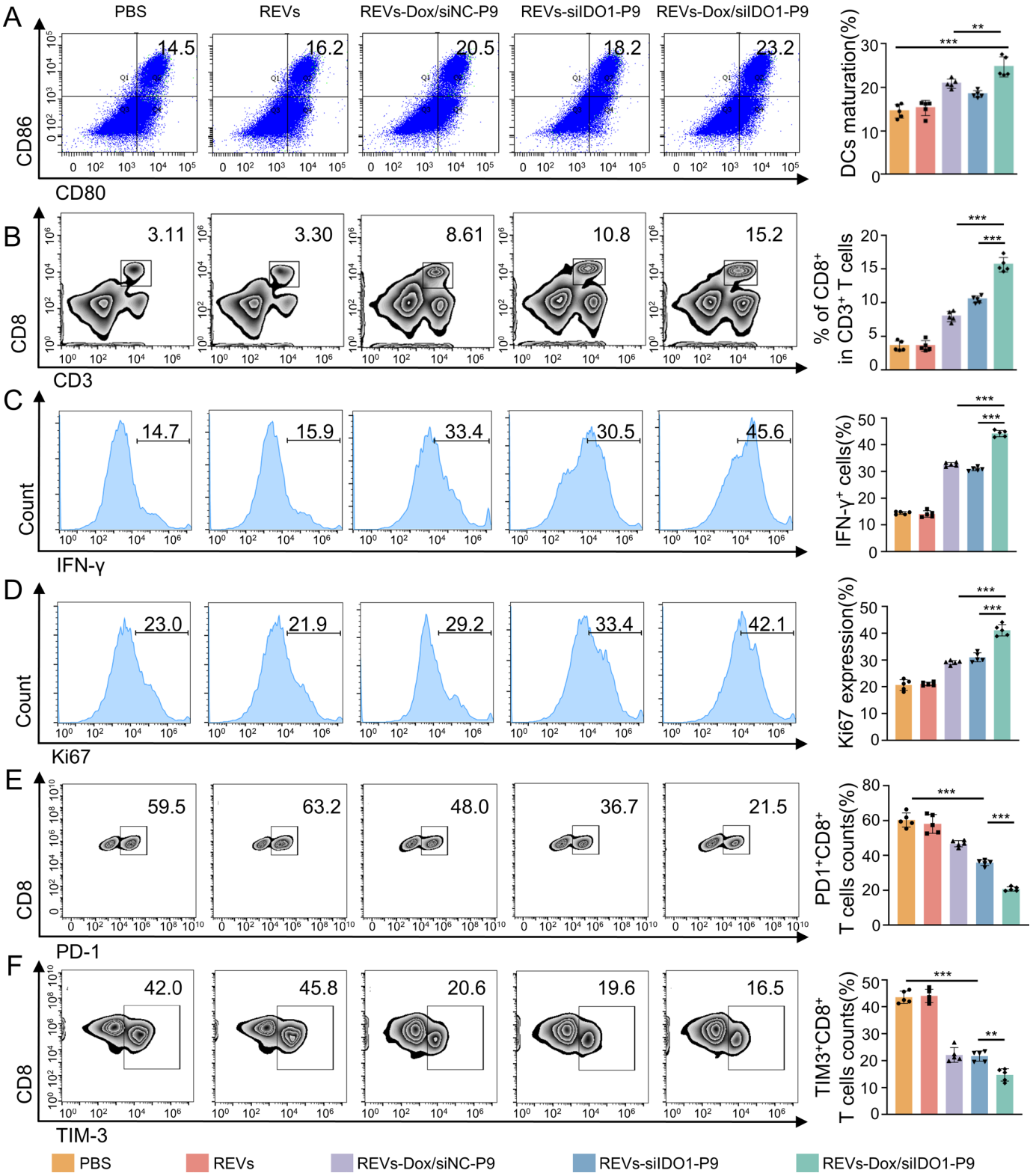

Figure 6 REVs-Dox/siIDO1-P9 promotes in vivo immune activation. (A) Mature DCs ($CD80^+CD86^+$) in draining lymph nodes were determined by flow cytometry (gated on $CD11c^+$ cells). (B) Flow cytometry analysis of $CD3^+CD8^+$ T cells infiltrating bone marrow from mice after administration with different formulations. (C,D) IFN-γ (C) and Ki67 (D) positive $CD8^+$ T cells in bone marrow from mice received different treatment. (E,F) Flow cytometry analysis showing PD-1 (E) and TIM-3 (F) expression of bone marrow $CD8^+$ T cells. Data were presented as mean±SD (n=5 mice per group). One-way ANOVA test in A–F. **p<0.01; ***p<0.001. ANOVA, analysis of variance; CD3, cluster of differentiation 3; CD8, cluster of differentiation 8; CD11c, cluster of differentiation 11 c; CD80, cluster of differentiation 80; CD86, cluster of differentiation 86; DCs, dendritic cells; Dox, doxorubicin; IDO1, indoleamine 2,3-dioxygenase-1; IFN-γ, interferon-gamma; Ki67, antigen KI-67; PD-1, programmed cell death protein-1; REVs, red blood cell-derived extracellular vesicles; TIM-3, T cell immunoglobulin and mucin-domain containing-3.

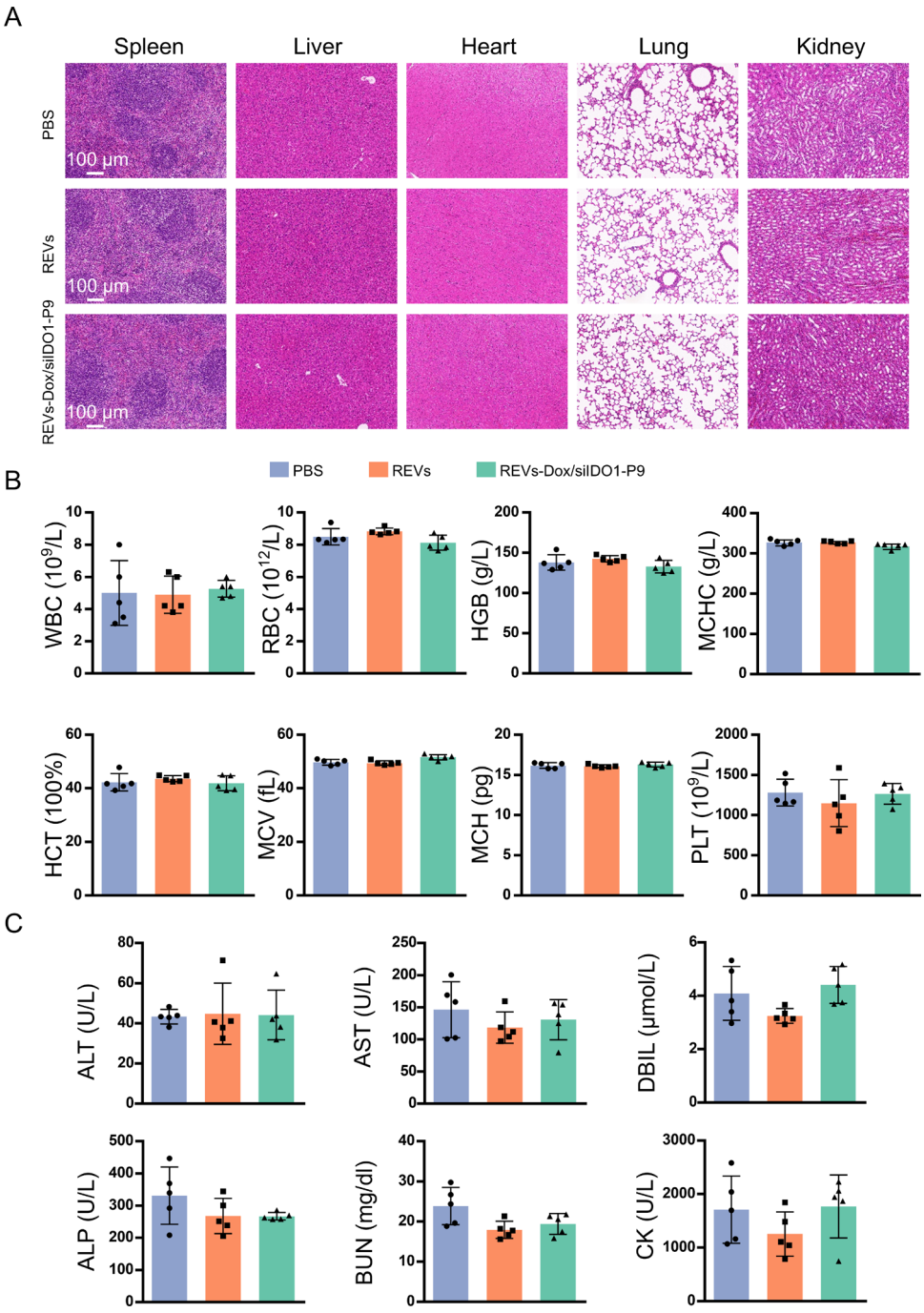

Figure 7 Biosafety assessment of REVs-Dox/siIDO1-P9 in vivo. (A) H&E analysis of tissues (spleen, liver, heart, lung, and kidney) from C57BL/6 mice injected with PBS, REVs, and REVs-Dox/siIDO1-P9. (B,C) The variations of blood routine test parameters (B) and serum biochemistry (C) for C57BL/6 mice in the indicated groups. Data were presented as mean±SD (n=5 mice per group). REVs, red blood cell-derived extracellular vesicles; Dox, doxorubicin; IDO1, indoleamine 2,3-dioxygenase-1; WBC,white blood cell; RBC, red blood cell; HGB, hemoglobin; HCT, hematocrit; MCV, mean corpuscular volume; MCH, mean corpuscular hemoglobin; MCHC, mean corpuscular hemoglobin concentration; PLT, platelet; ALT, alanine aminotransferase; AST, aspartate aminotransferase; DBIL, direct bilirubin; ALP, alkaline phosphatase; BUN, blood urea nitrogen; CK, creatine kinase.

horizontal gene transfer risk, are suitable for therapeutic delivery in disease treatment.[21 23] Our study demonstrated that using REVs as delivery vehicles results in an effective leukemia killing effect and immunomodulation without observable adverse effects, highlighting their potential for clinical application.

CONCLUSION

In summary, a REVs-based dual delivery biosystem (REVs-Dox/siIDO1-P9) has been developed to achieve a synergistic immune response in AML mice through chemo-immunotherapy. REVs derived from RBCs of blood group O, conjugated with targeting peptide P9,

were loaded with ICD inducer (Dox) and siIDO1. The biosystem specifically targeted leukemia cells, minimizing side effects. Importantly, the combined formulation could induce a potent adaptive antileukemia immunity by enhancing ICD induction, promoting DC maturation, relieving immunosuppression, and increasing the infiltration of antitumor $CD8^+$ T cells. Given the similar IDO1-mediated immunosuppression in solid tumors,[58 59] REVs-Dox/siIDO1 may show promise for treating other cancers as well. This study provides proof of concept for a synergistic chemo-immunotherapy approach in AML, transforming the tumor microenvironment into an immunefavorable state.

Author affiliations
[1]Key Laboratory of Laboratory Medical Diagnostics Designated by the Ministry of Education, College of Laboratory Medicine, Chongqing Medical University, Chongqing, China
[2]Department of Laboratory Medicine, Chongqing University Fuling Hospital, School of Medicine, Chongqing University, Chongqing, China
[3]Department of Hematology, The First Affiliated Hospital of Chongqing Medical University, Chongqing, China

Acknowledgements The authors thank Dr. Huan Li (Medical Center of Hematology, Xinqiao Hospital, Army Medical University, Chongqing, China) for help with manuscript revision.

Contributors YL, JH, YS, and LZ designed this study; YL, JH, JY, CL, NW, and MS performed the experiments; GL and LT analyzed the data; XW and JR organized the figures and drafted the initial manuscript; YL, FJ, XC, ZY, ZL, and LZ revised this manuscript; all authors read and approved the final manuscript. LZ is the guarantor.

Funding This work was supported by the National Natural Science Foundation of China (Grant No: 82072353) and the Natural Science Foundation of CQ CSTC (Grant No: CSTB2024NSCQ-MSX0167).

Competing interests None declared.

Patient consent for publication Not applicable.

Ethics approval Animal experiments were approved by the Ethics Committee of Chongqing Medical University and conducted according to the guidelines for the Care and Use of Laboratory Animals of Chongqing Medical University (IACUC-CQMU-2023-0295).

Provenance and peer review Not commissioned; externally peer reviewed.

Data availability statement Data are available upon reasonable request. The data and materials could be available from the corresponding author upon reasonable request.

ORCID iD
Ling Zhang http://orcid.org/0000-0003-1097-6034

REFERENCES

1 DiNardo CD, Erba HP, Freeman SD, *et al*. Acute myeloid leukaemia. *The Lancet* 2023;401:2073–86.
2 Yue S, An J, Zhang Y, *et al*. Exogenous Antigen Upregulation Empowers Antibody Targeted Nanochemotherapy of Leukemia. *Adv Mater Weinheim* 2023;35:e2209984.
3 Riley RS, June CH, Langer R, *et al*. Delivery technologies for cancer immunotherapy. *Nat Rev Drug Discov* 2019;18:175–96.
4 Laskowski TJ, Biederstädt A, Rezvani K. Natural killer cells in antitumour adoptive cell immunotherapy. *Nat Rev Cancer* 2022;22:557–75.
5 Loke J, Malladi R, Moss P, *et al*. The role of allogeneic stem cell transplantation in the management of acute myeloid leukaemia: a triumph of hope and experience. *Br J Haematol* 2020;188:129–46.
6 Vago L, Gojo I. Immune escape and immunotherapy of acute myeloid leukemia. *J Clin Invest* 2020;130:129204:1552–64:.
7 Galán-Díez M, Borot F, Ali AM, *et al*. Subversion of Serotonin Receptor Signaling in Osteoblasts by Kynurenine Drives Acute Myeloid Leukemia. *Cancer Discov* 2022;12:1106–27.
8 Prendergast GC, Malachowski WP, DuHadaway JB, *et al*. Discovery of IDO1 Inhibitors: From Bench to Bedside. *Cancer Res* 2017;77:6795–811.
9 Liu Y, Liang X, Dong W, *et al*. Tumor-Repopulating Cells Induce PD-1 Expression in $CD8^+$ T Cells by Transferring Kynurenine and AhR Activation. *Cancer Cell* 2018;33:480–94.
10 Rankin LC, Kaiser KA, de los Santos-Alexis K, *et al*. Dietary tryptophan deficiency promotes gut RORγt+ Treg cells at the expense of Gata3+ Treg cells and alters commensal microbiota metabolism. *Cell Rep* 2023;42:112135.
11 Cheong JE, Ekkati A, Sun L. A patent review of IDO1 inhibitors for cancer. *Expert Opin Ther Pat* 2018;28:317–30.
12 Wang Z, Li W, Jiang Y, *et al*. Sphingomyelin-derived nanovesicles for the delivery of the IDO1 inhibitor epacadostat enhance metastatic and post-surgical melanoma immunotherapy. *Nat Commun* 2023;14:7235.
13 Le Naour J, Galluzzi L, Zitvogel L, *et al*. Trial watch: IDO inhibitors in cancer therapy. *Oncoimmunology* 2020;9:1777625.
14 Wu C-C, Beird HC, Andrew Livingston J, *et al*. Immuno-genomic landscape of osteosarcoma. *Nat Commun* 2020;11:1008.
15 Zhou Y, Yang D, Yang Q, *et al*. Single-cell RNA landscape of intratumoral heterogeneity and immunosuppressive microenvironment in advanced osteosarcoma. *Nat Commun* 2020;11:6322.
16 Li Z, Lai X, Fu S, *et al*. Immunogenic Cell Death Activates the Tumor Immune Microenvironment to Boost the Immunotherapy Efficiency. *Adv Sci (Weinh)* 2022;9:2201734.
17 Chen L, Xue W, Cao J, *et al*. $TiSe_2$-mediated sonodynamic and checkpoint blockade combined immunotherapy in hypoxic pancreatic cancer. *J Nanobiotechnology* 2022;20:453.
18 Abdel-Bar HM, Walters AA, Lim Y, *et al*. An “eat me” combinatory nano-formulation for systemic immunotherapy of solid tumors. *Theranostics* 2021;11:8738–54.
19 Peng M, Ren J, Jing Y, *et al*. Tumour-derived small extracellular vesicles suppress CD8+ T cell immune function by inhibiting SLC6A8-mediated creatine import in NPM1-mutated acute myeloid leukaemia. *J Extracell Vesicles* 2021;10:e12168.
20 Zhang G, Huang X, Xiu H, *et al*. Extracellular vesicles: Natural liver-accumulating drug delivery vehicles for the treatment of liver diseases. *J Extracell Vesicles* 2020;10:e12030.
21 Usman WM, Pham TC, Kwok YY, *et al*. Efficient RNA drug delivery using red blood cell extracellular vesicles. *Nat Commun* 2018;9:2359.
22 Ye H, Minhajuddin M, Krug A, *et al*. The Hepatic Microenvironment Uniquely Protects Leukemia Cells through Induction of Growth and Survival Pathways Mediated by LIPG. *Cancer Discov* 2021;11:500–19.
23 Chen H, Jayasinghe MK, Yeo EYM, *et al*. CD33-targeting extracellular vesicles deliver antisense oligonucleotides against FLT3-ITD and miR-125b for specific treatment of acute myeloid leukaemia. *Cell Prolif* 2022;55:e13255.
24 Zheng G, Ma H-W, Xiang G-H, *et al*. Bone-targeting delivery of platelet lysate exosomes ameliorates glucocorticoid-induced osteoporosis by enhancing bone-vessel coupling. *J Nanobiotechnology* 2022;20:220.
25 Xu L, Xu X, Liang Y, *et al*. Osteoclast-targeted delivery of anti-miRNA oligonucleotides by red blood cell extracellular vesicles. *J Control Release* 2023;358:259–72.
26 Liang Y, Xu X, Xu L, *et al*. Chondrocyte-specific genomic editing enabled by hybrid exosomes for osteoarthritis treatment. *Theranostics* 2022;12:4866–78.

27 Zhang H, Yan W, Wang J, *et al*. Surface functionalization of exosomes for chondrocyte-targeted siRNA delivery and cartilage regeneration. *J Control Release* 2024;369:493–505.
28 Cao K, Du Y, Bao X, *et al*. Glutathione-Bioimprinted Nanoparticles Targeting of N6-methyladenosine FTO Demethylase as a Strategy against Leukemic Stem Cells. *Small* 2022;18:e2106558.
29 Peng B, Nguyen TM, Jayasinghe MK, *et al*. Robust delivery of RIG-I agonists using extracellular vesicles for anti-cancer immunotherapy. *J Extracell Vesicles* 2022;11:e12187.
30 Zhan Q, Yi K, Cui X, *et al*. Blood exosomes-based targeted delivery of cPLA2 siRNA and metformin to modulate glioblastoma energy metabolism for tailoring personalized therapy. *Neuro Oncol* 2022;24:1871–83.
31 Zhan Q, Yi K, Qi H, *et al*. Engineering blood exosomes for tumor-targeting efficient gene/chemo combination therapy. *Theranostics* 2020;10:7889–905.
32 Huang L, Rong Y, Tang X, *et al*. Engineered exosomes as an in situ DC-primed vaccine to boost antitumor immunity in breast cancer. *Mol Cancer* 2022;21:45.
33 Théry C, Witwer KW, Aikawa E, *et al*. Minimal information for studies of extracellular vesicles 2018 (MISEV2018): a position statement of the International Society for Extracellular Vesicles and update of the MISEV2014 guidelines. *J Extracell Vesicles* 2018;7:1535750.
34 Ismail M, Yang W, Li Y, *et al*. Biomimetic Dp44mT-nanoparticles selectively induce apoptosis in Cu-loaded glioblastoma resulting in potent growth inhibition. *Biomaterials* 2022;289:121760.
35 Wang Y, Huo Y, Zhao C, *et al*. Engineered exosomes with enhanced stability and delivery efficiency for glioblastoma therapy. *J Control Release* 2024;368:170–83.
36 Hemati M, Haghiralsadat F, Yazdian F, *et al*. Development and characterization of a novel cationic PEGylated niosome-encapsulated forms of doxorubicin, quercetin and siRNA for the treatment of cancer by using combination therapy. *Artif Cells Nanomed Biotechnol* 2019;47:1295–311.
37 Wang J, Chen S, Xiao W, *et al*. CAR-T cells targeting CLL-1 as an approach to treat acute myeloid leukemia. *J Hematol Oncol* 2018;11:7.
38 Liu Z, Xu X, Liu K, *et al*. Immunogenic Cell Death in Hematological Malignancy Therapy. *Adv Sci (Weinh)* 2023;10:2207475.
39 Wang Y, Gao D, Liu Y, *et al*. Immunogenic-cell-killing and immunosuppression-inhibiting nanomedicine. *Bioact Mater* 2021;6:1513–27.
40 He T, Wang L, Gou S, *et al*. Enhanced Immunogenic Cell Death and Antigen Presentation *via* Engineered *Bifidobacterium bifidum* to Boost Chemo-immunotherapy . *ACS Nano* 2023;17:9953–71.
41 Castellino A, Santambrogio E, Rapezzi D, *et al*. Atypical Chronic Myeloid Leukemia: New Developments from Molecular Diagnosis to Treatment. *Medicina (Kaunas)* 2021;57:1104.
42 MacNabb BW, Tumuluru S, Chen X, *et al*. Dendritic cells can prime anti-tumor $CD8^+$ T cell responses through major histocompatibility complex cross-dressing. *Immunity* 2022;55:982–97.
43 Pichler AC, Carrié N, Cuisinier M, *et al*. TCR-independent CD137 (4-1BB) signaling promotes $CD8^+$-exhausted T cell proliferation and terminal differentiation. *Immunity* 2023;56:1631–48.
44 Yang R, Sun L, Li C-F, *et al*. Galectin-9 interacts with PD-1 and TIM-3 to regulate T cell death and is a target for cancer immunotherapy. *Nat Commun* 2021;12:832.
45 Wang B, Chen J, Caserto JS, *et al*. An in situ hydrogel-mediated chemo-immunometabolic cancer therapy. *Nat Commun* 2022;13:3821.
46 Wei SC, Duffy CR, Allison JP. Fundamental Mechanisms of Immune Checkpoint Blockade Therapy. *Cancer Discov* 2018;8:1069–86.
47 Waldman AD, Fritz JM, Lenardo MJ. A guide to cancer immunotherapy: from T cell basic science to clinical practice. *Nat Rev Immunol* 2020;20:651–68.
48 Sharma P, Hu-Lieskovan S, Wargo JA, *et al*. Primary, Adaptive, and Acquired Resistance to Cancer Immunotherapy. *Cell* 2017;168:707–23.
49 DePeaux K, Delgoffe GM. Metabolic barriers to cancer immunotherapy. *Nat Rev Immunol* 2021;21:785–97.
50 Lim AR, Rathmell WK, Rathmell JC. The tumor microenvironment as a metabolic barrier to effector T cells and immunotherapy. *Elife* 2020;9:e55185.
51 Galluzzi L, Humeau J, Buqué A, *et al*. Immunostimulation with chemotherapy in the era of immune checkpoint inhibitors. *Nat Rev Clin Oncol* 2020;17:725–41.
52 Emens LA, Middleton G. The interplay of immunotherapy and chemotherapy: harnessing potential synergies. *Cancer Immunol Res* 2015;3:436–43.
53 Fukuno K, Hara T, Tsurumi H, *et al*. Expression of indoleamine 2,3-dioxygenase in leukemic cells indicates an unfavorable prognosis in acute myeloid leukemia patients with intermediate-risk cytogenetics. *Leuk Lymphoma* 2015;56:1398–405.
54 Folgiero V, Goffredo BM, Filippini P, *et al*. Indoleamine 2,3-dioxygenase 1 (IDO1) activity in leukemia blasts correlates with poor outcome in childhood acute myeloid leukemia. *Oncotarget* 2014;5:2052–64.
55 Chamuleau MED, van de Loosdrecht AA, Hess CJ, *et al*. High INDO (indoleamine 2,3-dioxygenase) mRNA level in blasts of acute myeloid leukemic patients predicts poor clinical outcome. *Haematologica* 2008;93:1894–8.
56 Mabuchi R, Hara T, Matsumoto T, *et al*. High serum concentration of L-kynurenine predicts unfavorable outcomes in patients with acute myeloid leukemia. *Leuk Lymphoma* 2016;57:92–8.
57 Corm S, Berthon C, Imbenotte M, *et al*. Indoleamine 2,3-dioxygenase activity of acute myeloid leukemia cells can be measured from patients' sera by HPLC and is inducible by IFN-γ. *Leuk Res* 2009;33:490–4.
58 Zhou Q-H, Han H, Lu J-B, *et al*. Up-regulation of indoleamine 2,3-dioxygenase 1 (IDO1) expression and catalytic activity is associated with immunosuppression and poor prognosis in penile squamous cell carcinoma patients. *Cancer Commun (Lond)* 2020;40:3–15.
59 Li A, Barsoumian HB, Schoenhals JE, *et al*. Indoleamine 2,3-dioxygenase 1 inhibition targets anti-PD1-resistant lung tumors by blocking myeloid-derived suppressor cells. *Cancer Lett* 2018;431:54–63.